Available online at www.sciencedirect.com
SCIENCE DIRECT
Journal of Catalysis 240 (2006) 47–57
JOURNAL OF CATALYSIS
www.elsevier.com/locate/jcat

Hydrothermal stability of CuZSM5 catalyst in reducing NO by NH_3 for the urea selective catalytic reduction process

Joo-Hyoung Park [a], Hye Jun Park [a], Joon Hyun Baik [a], In-Sik Nam [a,*], Chae-Ho Shin [b], Jong-Hwan Lee [c], Byong K. Cho [c], Se H. Oh [c]

[a] *Department of Chemical Engineering/School of Environmental Science and Engineering, Pohang University of Science and Technology (POSTECH), Pohang, Korea*
[b] *Department of Chemical Engineering, Chungbuk National University, Chungbuk, Korea*
[c] *General Motors R&D Planning Center, Warren, MI, USA*

Received 6 September 2005; revised 30 December 2005; accepted 6 March 2006

Available online 5 April 2006

Abstract

To confirm the hydrothermal stability of CuZSM5 for urea selective catalytic reduction (SCR), NO removal activity over a series of the catalyst containing various amounts of copper, ranging from 1 to 5 wt%, was examined before and after hydrothermal treatment under a simulated feed gas stream containing 10% water at a temperature range of 600–800 °C. The degree of catalyst aging varies with respect to the copper content of the catalyst and the aging temperature. The optimal copper content seems to be about 4 wt% (nearly 125% in terms of ion-exchange level) from the standpoint of catalyst aging. The catalysts before and after aging were characterized by XRD, ^{27}Al-MAS-NMR, BET, XAFS, and ESR to gain insight into the sintering mechanism of CuZSM5 for the urea SCR process. A slight alteration of the catalyst structure was observed by XRD and BET analysis on catalyst aging. The copper ions on the surface of CuZSM5 catalysts on aging remained as either isolated Cu^{2+} and/or an oxide form of copper, as confirmed by EXAFS. However, ESR spectra of the catalysts clearly revealed four distinct local structures of Cu^{2+} species in the framework of ZSM5 in the form of a square pyramidal site, a square planar site, and two unresolved distorted sites. Migration of Cu^{2+} ions from the square pyramidal and/or the square planar sites of the isolated cupric ions to the two unresolved sites occurs during hydrothermal treatment. This causes an alteration of the population of isolated cupric ions on the square pyramidal and/or planar sites and is responsible for the hydrothermal stability of the CuZSM5 catalyst in the urea SCR process.

Keywords: Urea SCR; Deactivation; Hydrothermal stability; ESR; XAFS; CuZSM5

1. Introduction

The selective catalytic reduction (SCR) of NO_x with urea is a recognized well-developed technology to remove NO_x from light- and heavy-duty diesel engines [1,2]. For the actual diesel engine exhaust system, the H_2O content generated from the combustion of diesel fuel with a high carbon number is distinctive in the gas stream, and the development of a hot spot in the catalytic converter from the sudden burning of locally collected particulate can be expected. Consequently, achieving hydrothermal stability of the catalyst is a critical issue in the commercial application of urea SCR technology to the exhaust stream from diesel engines [3].

CuZSM5 is one of the most promising catalysts for the SCR of NO_x by urea at an exhaust temperature of around 150 °C, particularly for light-duty diesel engines [3,4]. For the decomposition of urea, 1 mol of urea is thermally decomposed and then easily hydrolyzed on the catalyst surface to produce 2 mol of ammonia and 1 mol of carbon dioxide, leading to the practically equivalent overall reaction to NH_3 SCR of NO [3–7].

Numerous studies have been conducted regarding the nature of Cu on the surface of zeolite, which is generally recognized as an active reaction site for the present reaction system,

* Corresponding author. Fax: +82 54 279 8299.
E-mail address: isnam@postech.ac.kr (I.-S. Nam).

0021-9517/$ – see front matter
doi:10.1016/j.jcat.2006.03.001

and its reaction mechanism through redox chemistry [8–14]. It has been commonly accepted that isolated Cu^{2+} and Cu–O–Cu dimer species on the catalyst surface play key roles in the NH_3 SCR reaction. Mizumoto et al. [12] prepared Cu-Y zeolite containing mainly isolated Cu^{2+} to suggest a Langmuir–Hinshelwood-type reaction mechanism by the reaction between strongly adsorbed NH_3 and weakly adsorbed NO on isolated copper ions over the catalyst surface. Choi et al. also confirmed a similar mechanism by temperature-programmed desorption experiments of NO and NH_3 over Cu-exchanged Mordenite-type zeolite catalyst [13]. Komatsu et al. [14] studied NH_3 SCR for a series of Cu zeolites with varying copper exchange levels and Si/Al ratios and concluded that the active reaction site of the CuZSM5 catalyst for NH_3 SCR is copper dimer formed on the catalyst surface. The active reaction site on the surface of Cu-exchanged zeolite has been also investigated for the decomposition of NO and HC (hydrocarbon) SCR by luminescence, Fourier transform infrared spectroscopy, electron spin resonance (ESR), and X-ray absorption fine structure (XAFS) studies [15–23]. Iwamoto et al. proposed oxygen-bridged binuclear $[Cu–O–Cu]^{2+}$ in CuZSM5 for NO decomposition [15], and Sárkány et al. reported experimental evidence indicating that the complex forms all at once [16]. Ddeček et al. examined the four distinctive sites of Cu ion coordination over various zeolite structures, including MFI, MOR, FER, BEA, and FAU, using a multispectroscopic approach including Cu^{+} emission spectra, in situ infrared spectroscopy for Cu^{2+}-adsorbing NO, and ESR of Cu^{2+} [17].

But little literature exists on the inactivation of the active reaction sites for NH_3 SCR, although the hydrothermal stability of zeolite has long been considered a necessary issue to resolve for the commercial application of zeolite-type catalyst to automotive engines from the standpoint of alteration of the active reaction sites, including isolated Cu^{2+}, and Cu^{2+} dimer during the reaction. It has been commonly observed that the deactivation of SCR activity over CuZSM5 catalyst is due mainly to the degradation of zeolite support and/or the formation of Cu-aluminate by dealumination, the decrease in active reaction sites by the transformation of Cu^{2+} to CuO, the redistribution of the reaction sites through the migration of Cu^{2+}, or a combination of these mechanisms [19,20,24–28]. Furthermore, the optimal copper content on the catalyst surface has been little examined from the standpoint of catalyst aging for commercial application.

The purpose of the present study was to optimize the copper content on the surface of ZSM5 catalyst from the standpoint of catalyst aging by evaluating the hydrothermal stability of a series of CuZSM5 catalysts. To accomplish this goal, various complementary spectroscopic techniques were used and their results compared. In particular, XAFS and ESR studies were carried out to investigate the nature of copper ions on the surface of CuZSM5 catalyst, such as the oxidation states of copper and the coordination structure of Cu^{2+} in the framework of zeolite on the catalyst sintering with respect to aging temperature.

Table 1
Physicochemical properties of the catalysts employed in the present study

Sample	Cu content (wt%)	Ion exchange level (%)	BET (m^2/g)	Micropore surface area (m^2/g)
CuZSM5-61-fresh	1.95	61	400	377
CuZSM5-61-600				
CuZSM5-61-700			372	331
CuZSM5-61-800			363	321
CuZSM5-92-fresh	2.93	92	387	362
CuZSM5-92-600				
CuZSM5-92-700			357	319
CuZSM5-92-800			321	303
CuZSM5-124-fresh	3.87	124	383	354
CuZSM5-124-600			355	328
CuZSM5-124-700			324	285
CuZSM5-124-800				
CuZSM5-150-fresh	4.73	150	357	323
CuZSM5-150-600			337	301
CuZSM5-150-700			294	260
CuZSM5-150-800			191	182

2. Experimental

2.1. Catalyst preparation

NH_4^+ type ZSM5 (Si/Al ratio = 14), obtained from Tosoh Corp., was used as a parent catalyst for preparing the series of catalysts in the present study. The ZSM5 was exchanged with a 0.01 M $(CH_3CO_2)_2Cu{\cdot}H_2O$ (Aldrich, 98%) solution to obtain a Cu-based ZSM5 at room temperature for 5 h [3,4]. The room temperature for exchanging copper ions into ZSM5 catalyst was used to avoid the formation of copper oxides on the catalyst surface during the course of the ion exchange [4]. This was followed by drying at 110 °C for 12 h and calcining at 500 °C in air for 5 h. The copper content was controlled by repeating the ion-exchange procedure.

To investigate the hydrothermal stability of CuZSM5, the catalyst samples were sintered under a simulated feed gas stream containing 10% H_2O in air balance with a flow rate of 500 cc/min at 600, 700, and 800 °C for 24 h. Cu-based ZSM5 catalysts containing a various copper loadings with respect to the aging temperatures were obtained and designated as CuZSM5-*x*-*y*, where *x* and *y* represent the percentage degree of Cu^{2+} ion exchange, and the aging temperature, respectively. Table 1 lists the physicochemical properties of the catalysts prepared in this study.

2.2. Reactor system and experimental procedure

For urea SCR technology, urea is thermally decomposed into one mol of ammonia and one mol of isocyanic acid initially, and the isocyanic acid formed by the thermal decomposition of urea can readily undergo hydrolysis on the catalyst surface to produce another mol of ammonia [7]. Thus, the complete decomposition of 1 mol of urea produces 2 mol of ammonia and 1 mol of carbon dioxide [1,5–7],

$$H_2N–CO–NH_2 + H_2O \rightarrow 2NH_3 + CO_2. \quad (1)$$

This leads to the practically equivalent overall reaction of NO to NH_3 SCR. The identical deNO_x performance of the CuZSM5 catalyst by urea SCR to that by NH_3 SCR was observed under the specific reaction conditions [3]. Therefore, an NH_3 SCR test to confirm the hydrothermal stability of the series of the CuZSM5 catalysts for urea SCR was performed for experimental convenience.

The activity of the CuZSM5 catalysts for NO reduction by NH_3 was examined in a fixed-bed flow reactor, typically containing ca. 1 g of the catalyst was sieved to a mesh size of 20/30 to minimize the mass transfer limitations of the catalyst. Before the evaluation of activity, the catalyst was pretreated in situ with a total flow of 3300 cc/min containing 79% N_2 and 21% O_2 at 500 °C, and then cooled to room temperature. A reaction gas mixture consisting of 500 ppm NO, 500 ppm NH_3, 5% O_2, and 10% H_2O in N_2 balance was fed into the reactor system through Brooks mass flow controllers (model 5850E). A total flow rate of 3300 cc/min (corresponding to GHSV = 100,000 h^{-1}) was mainly used for the catalyst activity testing. The NO concentration was analyzed by an on-line chemiluminescence NO–NO_x analyzer (Thermo Electron, model 42H). The details of the reactor system have been given elsewhere [3,7].

2.3. Catalyst characterization

BET surface areas were measured by Micromeritics ASAP 2010 sorption analyzer with a static volumetric technique, based on the amount of N_2 adsorbed at liquid N_2 temperature. The samples were degassed at 200 °C in vacuum for 5 h before the adsorption measurements. BET surface area and micropore volume were calculated by the t-plot method. The micropore surface area was obtained by subtracting the external surface area from the total surface area.

Powder XRD patterns for the catalysts were observed by using an M18XHF X-ray diffractometer with Ni-filtered Cu-K_α radiation ($\lambda \sim 1.54184$ Å). Data were collected in angles ranging from 5° to 90° with a step size of 0.02° and a step time of 10 s under continuous sample rotation during the scan.

The ^{27}Al magic-angle spinning nuclear magnetic resonance (MAS-NMR) spectra were obtained on a Bruker AVANCE 500 spectrometer at an ^{27}Al frequency of 130.325 MHz in 4-mm rotors at a spinning rate of 10.0 kHz. The spectra were obtained with the acquisition of ca. 10,000 pulse transients, which were reported with a $\pi/4$ rad pulse length of 5.00 μs and a recycle delay of 1.0 s.

Extended X-ray absorption fine structure (EXAFS) spectroscopic measurements were performed with the synchrotron radiation by using the EXAFS facility installed at beamline 3C1 in the Pohang Accelerator Laboratory. The ring was operated at 2.5 GeV with 200 mA electron current and 1% coupling. The spectra were measured with an Si(111) channel-cut monochromator with an energy resolution of $\Delta E/E = 2 \times 10^{-4}$ that remained constant at the Cu K-edge (8979 eV).

The samples spread uniformly between adhesive tapes to obtain an optimal absorption jump. All of the data were recorded in a transmission mode at room temperature, and the intensities of the incident and transmitted beams were measured in 100% N_2-filled ionization chambers. CuO, Cu_2O, and Cu metal were used as reference compounds.

The data analyses for EXAFS were carried out by a standard procedure. The inherent background in the data was removed by fitting a polynomial to the edge region and then extrapolating through the entire spectrum from which it was subtracted. The resulting spectra, $\mu(E)$, were normalized to an edge jump of unity for comparing the X-ray absorption near-edge structures (XANES) directly. The EXAFS function, $\chi(E)$, was obtained from $\chi(E) = \{\mu(E) - \mu_0(E)\}/\mu_0(E)$ [29]. The resulting EXAFS spectra were k^2-weighted to compensate for the attenuation of EXAFS amplitude at high k and then Fourier transformed in the range of $2.0\ \text{Å}^{-1} \leqslant k \leqslant 11.5\ \text{Å}^{-1}$ with a Kaiser–Bessel function of $dk = 1\ \text{Å}^{-1}$. To determine the structural parameters, nonlinear least squares curve fitting was performed in the range of $R \leqslant \sim 2$ Å corresponding to the distance to the Cu–O in the central-atom phase-corrected Fourier-transformed (FT) spectra, using the UWXAFS and IFEFFIT packages according to the following EXAFS formula [30]:

$$\chi(k) = -S_0^2 \sum_i \frac{N_i}{kR_i^2} F_i(k) \exp\{-2\sigma_i^2 k^2\} \exp\{-2R_i/\lambda(k)\} \times \sin\{2kR_i + \phi_i(k)\}, \quad (2)$$

where the backscattering amplitude, $F_i(k)$, the total phase shift, $\phi_i(k)$, and the photoelectron mean free path, $\lambda(k)$, were theoretically calculated for all scattering paths, including multiple ones by a curved wave ab initio EXAFS code FEFF8 [31].

The ESR spectra were obtained at room temperature in the X-band using a JEOL model JES-TE300 spectrometer. The ESR signals of Cu^{2+} were recorded in the field region from 2000 to 4000 G with a sweep time of 10 min. A coaxial quartz cell was placed in the ESR cavity and connected with stainless steel capillaries of the flow system by Teflon ferrules. The samples were heated at 500 °C in pure O_2, evacuated, and sealed off in situ. To provide the maximum accuracy of the ESR signals, the packing height of the ampoule was constant in all cases, with the center of the sample positioned in the middle of the ESR cavity. The ESR signal from DPPH ($g_\parallel = 2.0036$) was used as an internal standard. The Origin and Excel programs for Windows were used for the baseline correction, analysis of the fourfold hyperfine lines, and double-integration of the recorded ESR spectra.

3. Results and discussion

3.1. Effect of aging on NO removal activity

The NO removal activity for a series of CuZSM5 catalysts before and after aging, particularly at 700 °C, where catalyst deactivation is specifically evident, is given in Fig. 1. The figure shows a bell-shaped activity profile with respect to the reaction temperature, typical for NH_3 SCR catalyst maintaining a wide operating temperature window (200–400 °C) containing NO conversion >90%. In a reaction temperature range higher than 400 °C, NO conversion gradually decreases mainly due to

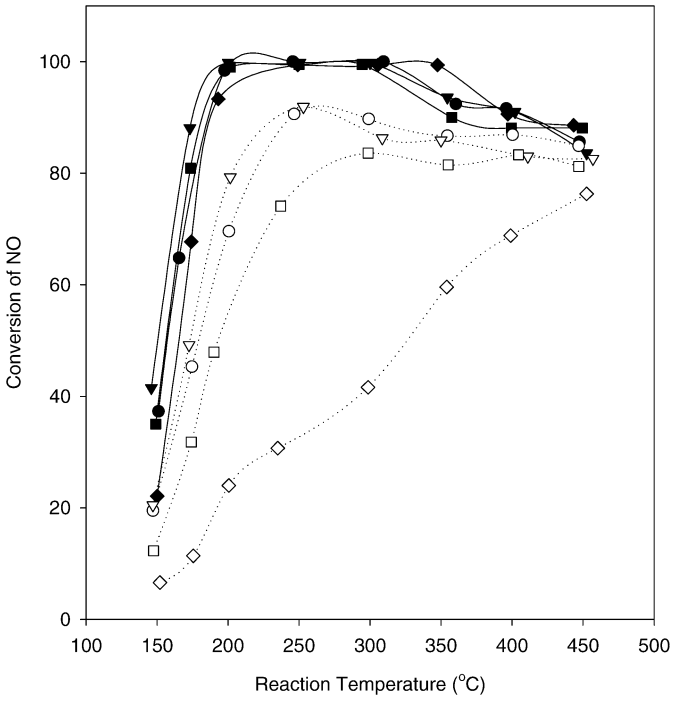

Fig. 1. Activity of a series of CuZSM5 catalysts before and after aging at 700 °C [(◆) CuZSM5-61-fresh, (■) CuZSM5-92-fresh, (▼) CuZSM5-124-fresh, (●) CuZSM5-150-fresh, (◇) CuZSM5-61-700, (□) CuZSM5-92-700, (▽) CuZSM5-124-700, (○) CuZSM5-150-700] for the reduction of NO by NH_3. Feed gas composition is 500 ppm NO, 500 ppm NH_3, 5% O_2, 10% H_2O in N_2 balance.

the oxidation of NH_3 at the high reaction temperature with oxygen leading to a significant decrease in NH_3 selectivity for NO_x reduction as follows [32]:

$$4NH_3 + 3O_2 \rightarrow 2N_2 + 6H_2O. \quad (3)$$

Among the catalysts before and after aging, CuZSM5-124 exhibited the best performance for NO removal activity maintenance, even at a reaction temperature below 200 °C, which is critical for the application of the present urea SCR technology to light-duty diesel engines. However, the activity for underexchanged CuZSM5-61 catalyst aged at 700 °C decreases significantly.

Figs. 2 and 3 illustrate the aging effect of a series of CuZSM5 catalysts with respect to the copper content and the aging temperatures on NO removal activity in a reaction temperature range of 150–450 °C. For the catalysts containing <4% copper loading, NO removal activity increases as the Cu loading increases, regardless of the catalyst aging. However, for a highly overexchanged catalyst such as CuZSM5-150, the activity decrease due to the catalyst sintering is somewhat milder than that for slightly overexchanged catalyst, CuZSM5-124. For an underexchanged catalyst containing low copper content, such as CuZSM5-65, the worst catalyst deactivation can be observed, even for the catalyst aged at 600 °C. However, the cause of the sintering of Cu-based zeolite catalyst for SCR reaction has not yet been systematically examined. It has been simply speculated, probably due to the structural destruction of thezeolite, and the alteration of the chemical state of copper on the catalyst surface [19,20,24–28].

3.2. Confirming the structure of the catalyst support, ZSM5, by ^{27}Al MAS-NMR and powder XRD

^{27}Al MAS-NMR spectra were examined for the CuZSM5-150 catalyst before and after hydrothermal treatment with the simulated aging gas stream containing 10% water, as shown in Fig. 4. No shoulder due to extra-framework AlO_4 units was detected even for CuZSM5-150-800, except for that assigned to tetrahedral Al species. It may be direct evidence for the maintenance of the catalyst structure without dealumination from the framework of zeolite due to hydrothermal treatment even at 800 °C. Identical NMR results were observed for all of the catalysts before and after aging. However, the intensity of the Al tetrahedral peak decreased, as also shown in Fig. 4, probably due to the paramagnetic field of the Cu ions at their ion-exchange positions in the framework of zeolite structure. This characteristic of the Cu ions also produces an intensified and extended side band of the NMR spectra, which may be originated from the anisotropic dipolar interaction between the electron spin of the Cu ions and the nuclei spin of the Al in the zeolite framework [33].

Fig. 5 shows the typical powder XRD patterns for the series of the catalysts prepared before and after hydrothermal treatment. The relative intensities of X-ray peaks decrease due to the amount of Cu loadings on the catalyst surface and the aging temperature, particularly for underexchanged CuZSM5 catalysts. In addition, a fairly obvious weaker crystallinity for the overexchanged CuZSM5 compared with the underexchanged one is seen. It closely agrees with the decreasing trends of BET and micropore surface areas on the hydrothermal treatment of the catalysts as listed in Table 1. The irreversible decrease of the catalyst surface areas mainly causes a permanent loss of NO removal activity for overexchanged CuZSM5 catalysts aged at the high sintering temperature. It may be also attributed to the simultaneous effects of the combination of high Cu loading and harsh aging conditions on the framework structure of ZSM5-type zeolite catalyst [34]. In addition, a broad XRD peak can be observed at 2θ of ca. 35.5° and 39° in the patterns of CuZSM5-150 catalysts, indicating formation of CuO on the catalyst surface, even for the fresh counterpart catalyst, but basically no CuO peak for the slightly underexchanged CuZSM5 catalyst, regardless of the aging temperatures. This may cause the decrease of NO removal activity of overexchanged CuZSM5 catalyst aged at 800 °C, as mentioned earlier, but catalyst deactivation for underexchanged CuZSM5 catalysts can barely be elucidated. Note that the additional XRD peaks for the formation of CuO and Cu_2O on the catalyst surface of underexchanged CuZSM5 also cannot be identified, as shown in Fig. 5. Also note that formation of the Cu-aluminate related to the octahedral Al of the catalyst was hardly observed on the basis of the ^{27}Al MAS-NMR and XRD results, although we did not conduct a TPR analysis to confirm its formation, as was done by Yan et al. [28].

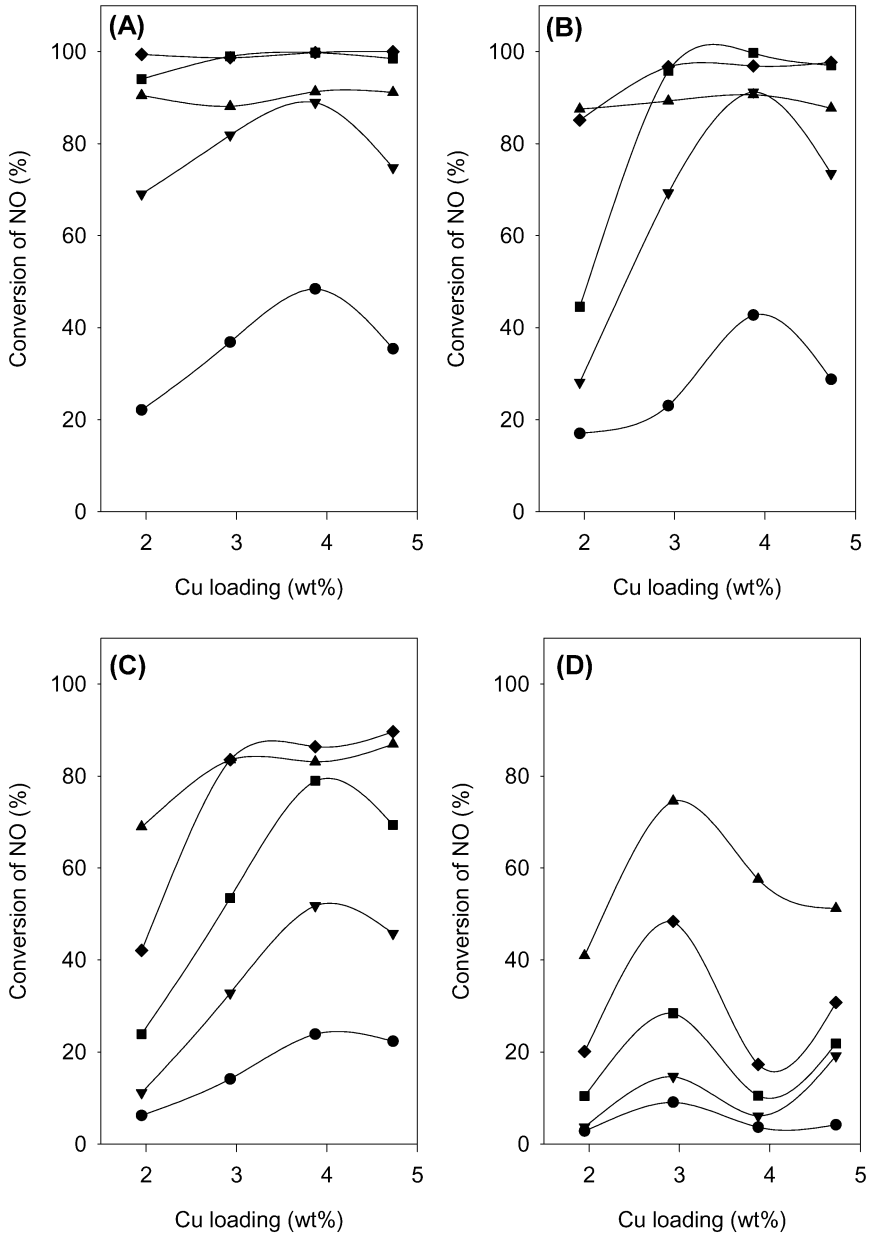

Fig. 2. Effect of Cu loading on the conversion of NO for CuZSM5 catalysts: (A) fresh, (B) aged at 600 °C, (C) aged at 700 °C, and (D) aged at 800 °C. Feed gas composition is 500 ppm NO, 500 ppm NH_3, 5% O_2, 10% H_2O in N_2 balance, and SV is 100,000 h^{-1}. [Reaction temperature: (●) 150, (▼) 175, (■) 200, (◆) 300, and (▲) 400 °C.]

3.3. Local structure of copper ions by XAFS

The shape and position of the Cu *K*-edge XANES provide information on the electronic structure and the local coordination geometry of the absorbing Cu atom [22–24,35–42]. Fig. 6 shows the XANES spectra for CuZSM5 catalysts, which are quite typical for the existence of the distorted octahedral Cu^{2+} on the catalyst surface. The first derivatives of the XANES spectra for the catalyst samples on the hydrothermal treatment are given in Fig. 7; the general patterns are basically identical. In fact, the weak pre-edge peaks (I), corresponding to an electric dipole-forbidden, but quadruply and vibronically allowed 1s → 3d electronic transition and providing direct information on the oxidation state of copper, can be observed at ca. 8979 eV, which is the fingerprint of Cu^{2+} species on the catalyst surface [23,36].

The primary absorption peaks (II and III) for all of the catalysts appear at ca. 8986–8988 and 8995–8998 eV, respectively, which are attributed to the charge transfer from the metal ligand to the 3d orbital (ligand-to-metal charge transfer) corresponding to the degree of Cu(3d)–O(2p) bond covalence, and 1s → 4p transition, respectively [23,36]. The shift of peak positions has been also observed at the lower absorption energy. The evolution of the absorption peaks (II and III) in Fig. 7 with respect to the Cu content and the aging condition may be due to the gradual polymerization of Cu^{2+} ions with oxygen ion (O^{2-}) on the catalyst surface. To identify and evaluate the peak position of the absorption edge (E_0) defined as the maximum of the

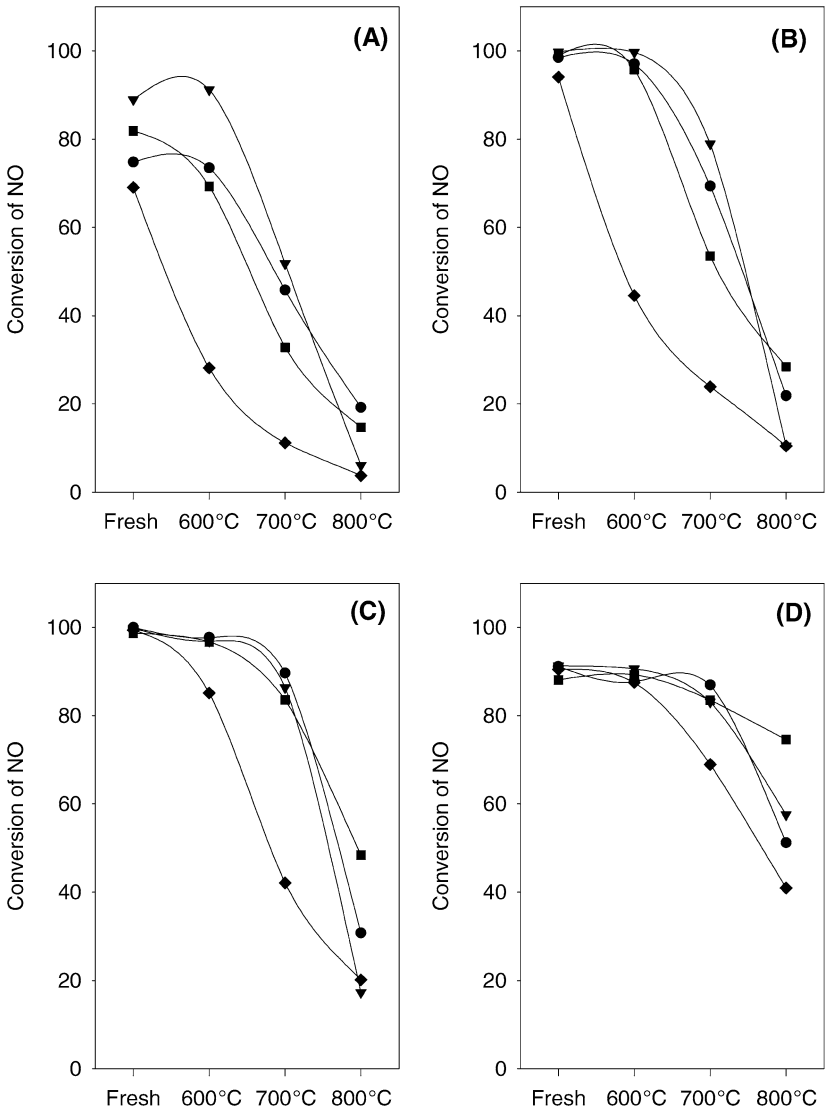

Fig. 3. Effect of aging temperatures on the conversion of NO for CuZSM5 catalysts at reaction temperatures of (A) 175, (B) 200, (C) 300, and (D) 400 °C. Feed gas composition is 500 ppm NO, 500 ppm NH_3, 5% O_2, 10% H_2O in N_2 balance, and SV is 100,000 h^{-1} [(◆) CuZSM5-61, (■) CuZSM5-92, (▼) CuZSM5-124, (●) CuZSM5-150].

first derivative of XANES spectra for CuZSM5 catalysts, the references including CuO, Cu_2O, and Cu metal have been also analyzed and compared as listed in Table 2, where the apparent trend of the shift to the lower absorption energy can be seen.

For the catalysts aged at the harshest sintering temperature of 800 °C except CuZSM5-61, an additional peak (IV) appears at ca. 8984 eV, which is due to the transition of copper ion into the bulk-type CuO [23]. It indicates that the copper on the surface of the catalyst can be transferred to a crystalline CuO by the hydrothermal treatment. These results were reconfirmed by EXAFS studies on the state of Cu on the catalyst surface.

It has been generally recognized that EXAFS is an effective tool for evaluating interatomic distances and coordination numbers to explore the geometric structure of reaction sites, due mainly to the interaction between an absorbing atom and a nearly surrounding atom [22,23,36,39,40]. Fig. 8 shows the radial distribution functions (RDFs) of Cu of CuZSM5 catalysts with CuO as a reference compound by Cu K-edge k^2-

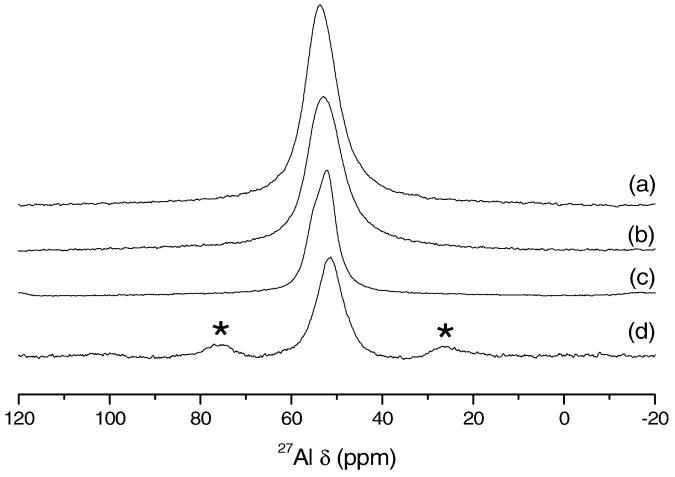

Fig. 4. ^{27}Al-MAS-NMR spectra of CuZSM5-150 before and after aging: (a) fresh, (b) aged at 600, (c) 700, and (d) 800 °C [∗ symbol indicating spinning sidebands].

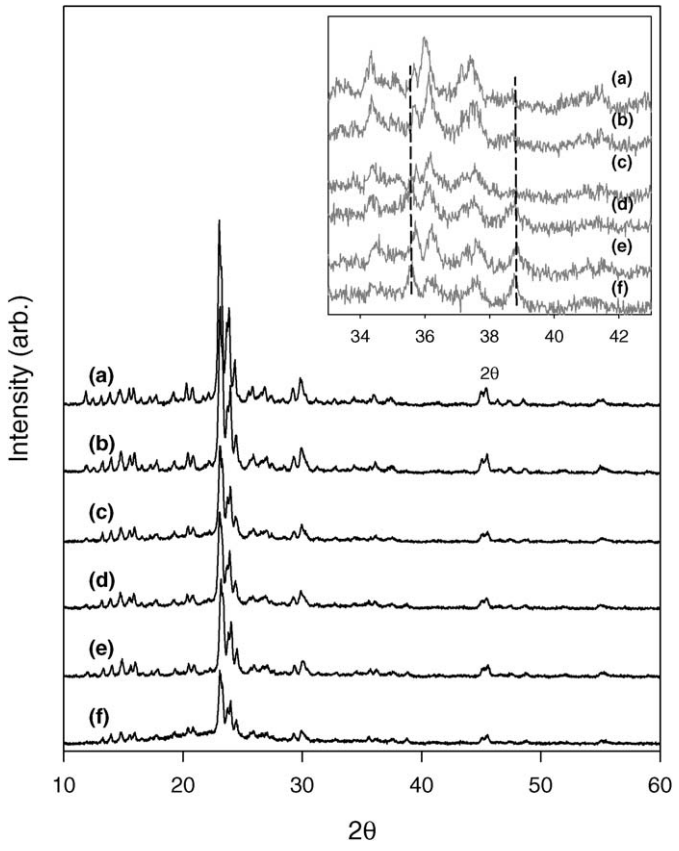

Fig. 5. XRD patterns of the under-exchanged (CuZSM5-92) and over-exchanged (CuZSM5-150) before and after aging. (a) CuZSM5-92-fresh, (b) CuZSM5-92-700, (c) CuZSM5-92-800, (d) CuZSM5-150-fresh, (e) CuZSM5-150-700, and (f) CuZSM5-150-800. (Inset figure is a detailed XRD patterns for the identical catalysts ranged from 33° to 43° of the diffraction angle and the dashed lines are the characteristic peak positions of bulk CuO.)

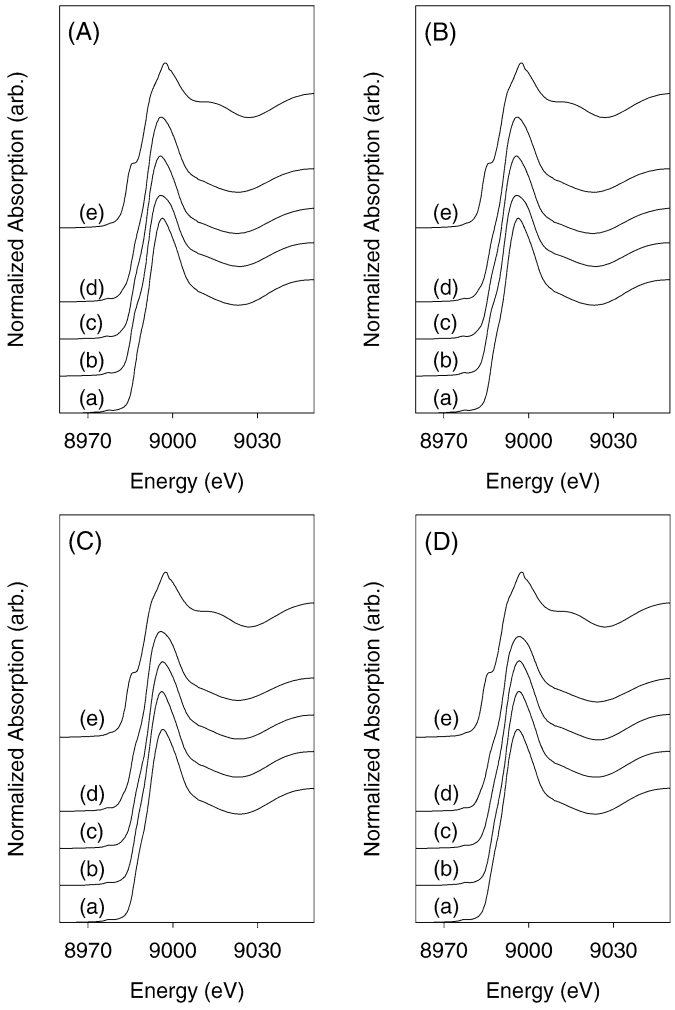

Fig. 6. Cu K-edge XANES spectra for CuZSM5 catalysts before and after aging: (A) CuZSM5-61, (B) CuZSM5-92, (C) CuZSM5-124, and (D) CuZSM5-150 [(a) fresh, (b) aging at 600 °C, (c) aging at 700 °C, (d) aging at 800 °C, and reference (e) CuO].

weighted Fourier transforms (FTs) in the range of 2.0 $\text{Å}^{-1} \leqslant k \leqslant 11.5\ \text{Å}^{-1}$ with a Kaiser–Bessel function. Dominant spectra with a Cu–O distance of ca 1.96 Å were commonly observed for the catalysts examined in this study [22,23]. As clearly shown in Fig. 9, the best fits of the EXAFS data for the CuZSM5 samples were attained; their parameters are summarized in Table 2. It is noteworthy that the coordination number of the Cu–O shell for CuZSM5 samples decreases with respect to the aging temperatures from 600 to 800 °C, indicating that Cu^{2+} ion may migrate to the inaccessible sites or transform isolated Cu^{2+} ions into small CuO-like phases.

An additional weak Cu–(O)–Cu bond at ca. 2.95 Å [23] was seen for all but the underexchanged catalysts, including CuZSM5-61 and CuZSM5-92-fresh, due to the local structure of crystalline CuO formed on the catalyst surface. The amplitude of the Cu–(O)–Cu peak for the CuZSM5 catalyst was much weaker than that for the bulk oxides, with coordination number <4 [23]. As the aging condition became more severe and the Cu loading content increased, the amplitude of the peak became evident. For highly overexchanged ZSM5 catalysts, a Cu–(O)–Cu peak was observed even for its fresh counterpart. It may be concluded that Cu zeolites prepared by the solution ion-exchange method can contain Cu–O–Cu dimeric oxocations that may be transferred to crystalline CuO as catalyst aging proceeds and/or the Cu loading content of the catalyst increases. Although the XAFS studies can examine the oxidation state of copper on the catalyst surface, the interatomic distance, and the coordination number of copper ion on the surface of CuZSM5 catalyst to characterize the geometric structure of the Cu atoms, it may not be sufficient to clearly assess the characteristics of Cu^{2+} species, the amount of the isolated Cu^{2+}, the degree of transformation of Cu^{2+} into bulk-type CuO, and other features that may be critical to elucidate the aging mechanism of CuZSM5 catalyst to remove NO from automotive diesel engine by urea.

3.4. Migration of copper among the reaction sites over the catalyst on aging

To examine the alteration of the local characteristics of Cu^{2+} ions by sintering, the CuZSM5 catalysts before and after hydrothermal treatment were pretreated in situ at 500 °C for 2 h in pure O_2 flow, evacuated, and sealed off for ESR study [22]. To

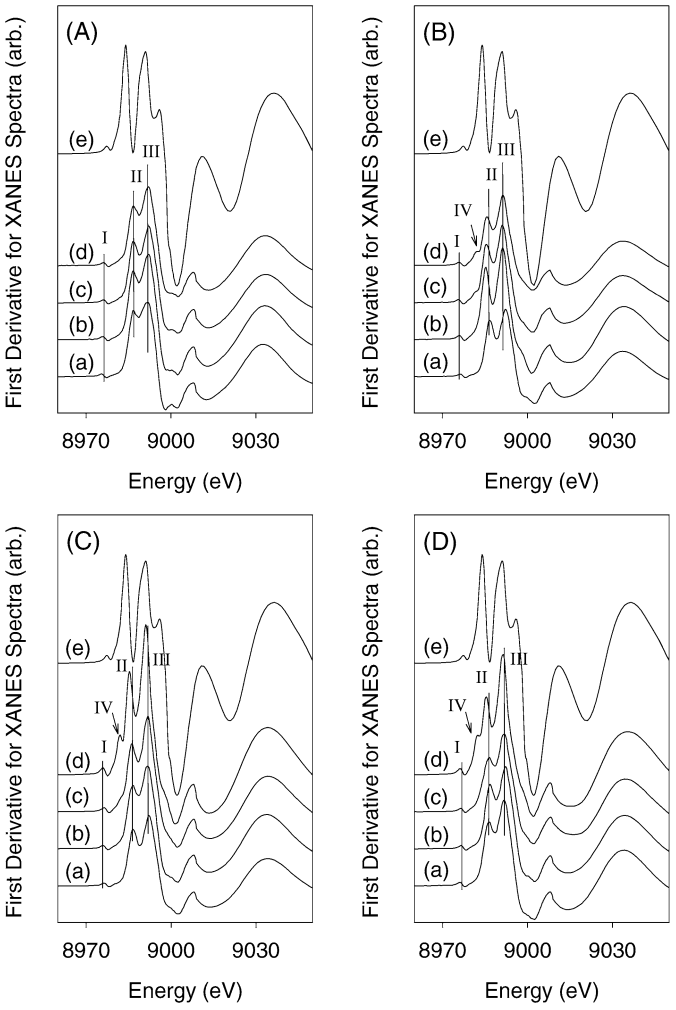

Fig. 7. First-derivative of XANES spectra for CuZSM5 catalysts before and after aging: (A) CuZSM5-61, (B) CuZSM5-92, (C) CuZSM5-124, and (D) CuZSM5-150 [(a) fresh, (b) aging at 600 °C, (c) aging at 700 °C, (d) aging at 800 °C, and reference (e) CuO].

obtain better resolution of ESR spectra and investigate the effect of measurement temperature on the state of Cu ions in the framework of the ZSM5 catalyst, the ESR studies were conducted at both room temperature and liquid nitrogen temperature. No significant variation of the ESR spectra was observed. Fig. 10 shows the X-band ESR spectra for the CuZSM5-125 catalysts, an axially symmetrical signal split into four hyperfine lines that can be resolved as the parallel component of ESR spectra. This fourfold hyperfine splitting of the spectra was caused by the coupling between the 3d unpaired electron and the copper ($I = 3/2$) nuclear spin. For an orientationally disordered solid assuming axial symmetry, g anisotropy produces a powder pattern in which the sharp features are referred to as parallel and perpendicular edges [20,22,24,41,42].

The spectra of fresh samples exhibited two characteristic perpendicular g values: Cu^{2+} in a square planar environment (by $g_{\parallel} = 2.27$–2.30 and $A_{\parallel} = 150$–170 G) and square pyramidal ($g_{\parallel} = 2.33$–2.35 and $A_{\parallel} = 135$–145 G) [20,22,24,41,42]. For CuZSM-5 catalysts after aging, two additional Cu^{2+} species, containing $g_{\parallel} = 2.30$ and $A_{\parallel} = 165$ G and $g_{\parallel} = 2.36$ and $A_{\parallel} = 130$ G of ESR signals, have been found on the catalyst surface [20,24]. The exact geometry of the third and fourth Cu^{2+} species is not completely understood, however.

Table 2
Cu K-edge EXAFS least-square fitting results in CuZSM5 samples with respect to copper loadings and aging temperatures

Sample	C.N.[a]	R_{eff}[b]	ΔE[c]	Sigma[d]	R-factor	Edge energy[e]
CuZSM5-61-fresh	5.3	1.976	−6.6	0.0040	0.0010	8992.2
CuZSM5-61-600	4.9	1.960	−7.7	0.0040	0.0030	8992.2
CuZSM5-61-700	5.1	1.959	−8.3	0.0049	0.0053	8993.2
CuZSM5-61-800	4.9	1.957	−7.8	0.0044	0.0055	8992.2
CuZSM5-92-fresh	5.6	1.956	−7.5	0.0057	0.0060	8991.6
CuZSM5-92-600	4.9	1.955	−6.4	0.0047	0.0017	8990.8
CuZSM5-92-700	5.1	1.952	−7.2	0.0053	0.0042	8991.0
CuZSM5-92-800	3.9	1.947	−7.4	0.0021	0.0137	8991.6
CuZSM5-124-fresh	5.4	1.955	−7.1	0.0053	0.0031	8991.6
CuZSM5-124-600	5.3	1.951	−7.3	0.0050	0.0042	8990.8
CuZSM5-124-700	5.0	1.954	−6.8	0.0054	0.0055	8991.8
CuZSM5-124-800	3.8	1.956	−5.2	0.0015	0.0137	8990.6
CuZSM5-150-fresh	5.1	1.955	−7.1	0.0048	0.0025	8991.6
CuZSM5-150-600	5.5	1.954	−7.6	0.0057	0.0025	8992.2
CuZSM5-150-700	5.3	1.959	−6.6	0.0050	0.0022	8991.8
CuZSM5-150-800	4.6	1.947	−6.4	0.0050	0.0020	8991.4

[a] Coordination number.
[b] Energy shift.
[c] Interatomic distance.
[d] Debye–Waller factor.
[e] Determined from the position of the maximum of the derivative of XANES spectra for the samples.

Based on the ESR parameters examined in the present study, the third species ($g_{\parallel} = 2.30$ and $A_{\parallel} = 165$ G) obtained over the aged catalyst can be coordinated to a distorted square sites anchored on the locations recessed from the main channels (i.e., in the side pockets of the zeolite structure), and the fourth species ($g_{\parallel} = 2.36$ and $A_{\parallel} = 130$ G) can be assigned to slightly distorted octahedral [20,43]. A recessed location would be expected to alter the redox cycle of copper presumably during the SCR of NO_x by impairing the accessibility of the reactants, hence decreasing the overall NO removal activity [18,42]. Similar results were also observed for the CuZSM5 catalysts with differing copper contents. The g and hyperfine interaction constant values listed in Table 3 are nearly identical to those reported earlier for CuZSM5 [20,24].

Double-integral (DI) values of ESR spectra for CuZSM5 catalysts were obtained for a comparative study to quantify the number of active Cu species on the catalyst surface, assuming the isolated Cu^{2+} ions as the active reaction sites [22,42] for NO removal activity by NH_3 SCR; these are given in Table 4. The altered number of reaction sites may be represented by the relative percentage of DI values of the ESR spectra for CuZSM5 catalysts, where the absorption area of ESR spectrum for CuZSM5-92-fresh is used as a basis for the calculation to confirm the migration of the copper ions among the reaction sites, an arbitrary criterion set for this comparative study. The relative percentages of DI values for fresh CuZSM5 catalyst

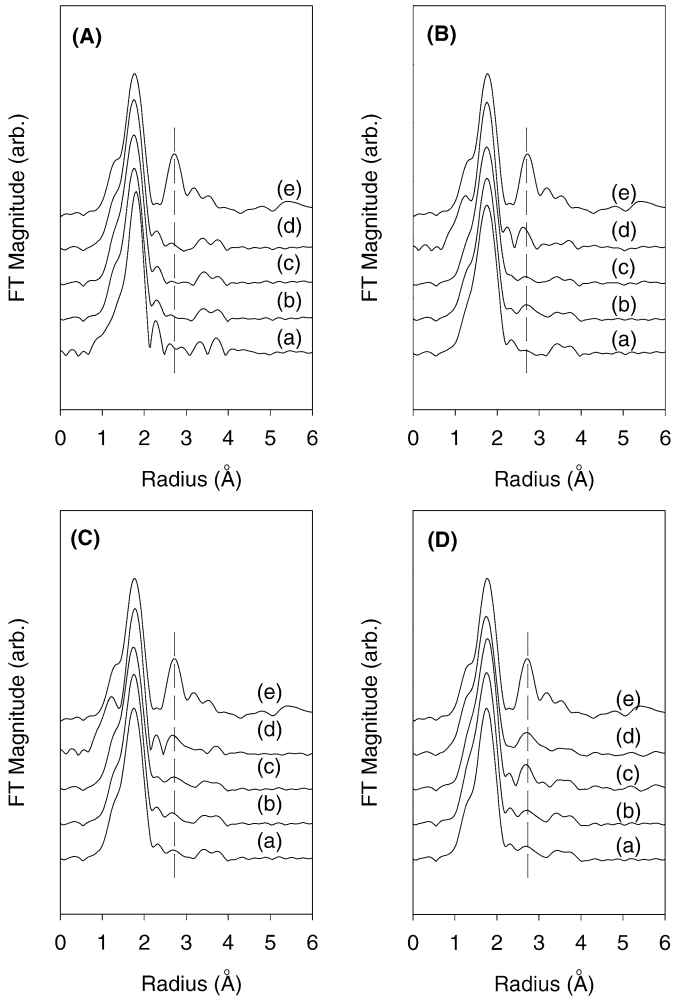

Fig. 8. EXAFS RDF of Cu K-edge for CuZSM5 catalysts before and after aging: (A) CuZSM5-61, (B) CuZSM5-92, (C) CuZSM5-124, and (D) CuZSM5-150 [(a) fresh, (b) aging at 600 °C, (c) aging at 700 °C, and (d) aging at 800 °C, (e) CuO].

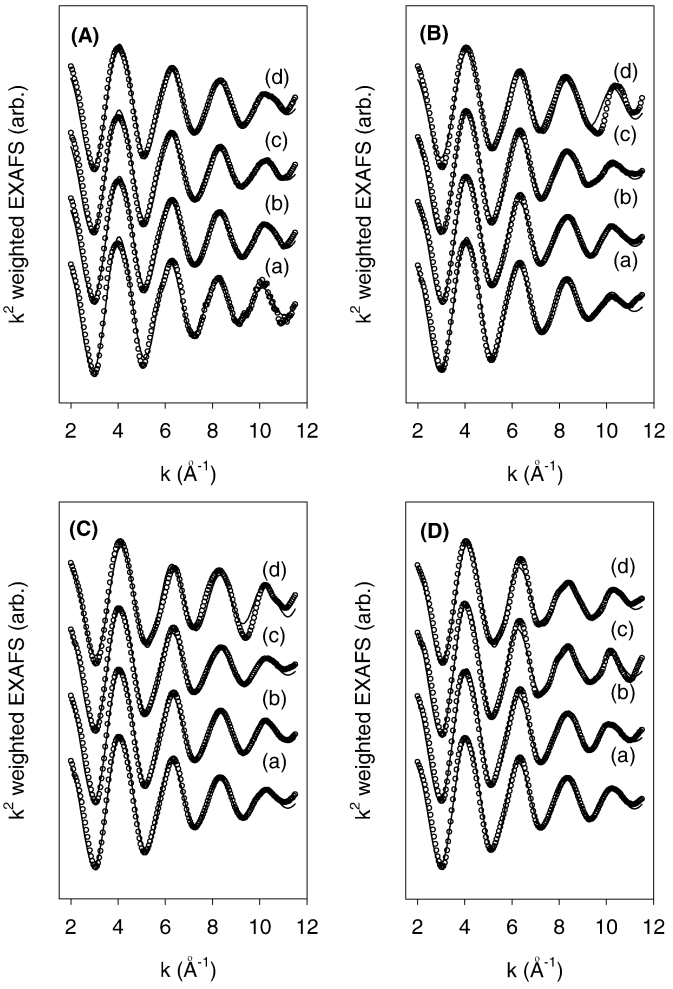

Fig. 9. Cu K-edge k^2 weighted EXAFS data (○) and their best fits (–) for CuZSM5 catalysts before and after aging: (A) CuZSM5-61, (B) CuZSM5-92, (C) CuZSM5-124, and (D) CuZSM5-150 [(a) fresh, and aging at (b) 600, (c) 700, and (d) 800 °C].

Table 3
ESR parameters ($g_\parallel$, $A_\parallel$) determined for a series of CuZSM5 samples ($A_\parallel$ is given in Gauss)

Sample	$g_\parallel$ [a]	$A_\parallel$ [a]	$g_\parallel$ [b]	$A_\parallel$ [b]	$g_\parallel$ [c]	$A_\parallel$ [c]	$g_\parallel$ [d]	$A_\parallel$ [d]
CuZSM5-61-fresh	2.29	150						
CuZSM5-61-700	2.29	150	2.34	135	2.30	165	2.37	130
CuZSM5-61-800			2.34	135	2.30	165	2.37	130
CuZSM5-92-fresh	2.30	153	2.35	140				
CuZSM5-92-700	2.30	153	2.35	140	2.30	165	2.36	130
CuZSM5-92-800	2.30	153	2.35	140	2.30	165	2.36	130
CuZSM5-124-fresh			2.33	145				
CuZSM5-124-700			2.33	145	2.30	165	2.36	130
CuZSM5-124-800	2.29	155	2.33	145	2.30	165	2.36	130
CuZSM5-150-fresh			2.34	142				
CuZSM5-150-700			2.34	142	2.30	165	2.36	130
CuZSM5-150-80	2.29	155	2.34	142	2.30	165	2.36	130

[a] Square planar site.
[b] Square pyramidal site.
[c] Unresolved site (distorted square pyramidal).
[d] Unresolved site (distorted octahedral).

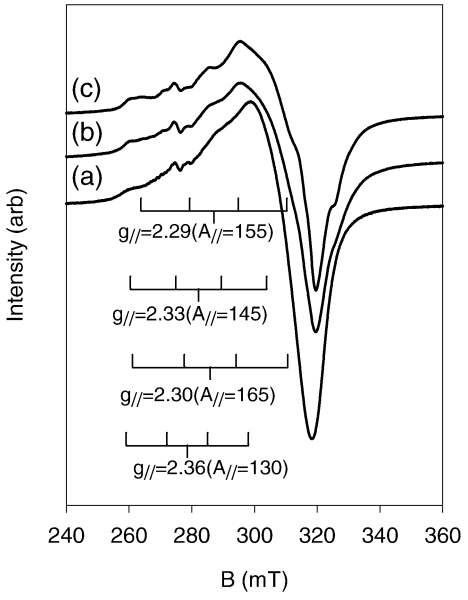

Fig. 10. ESR spectra on CuZSM5-124 catalysts before and after aging: (a) fresh, and aging at 700 (b) and (c) 800 °C.

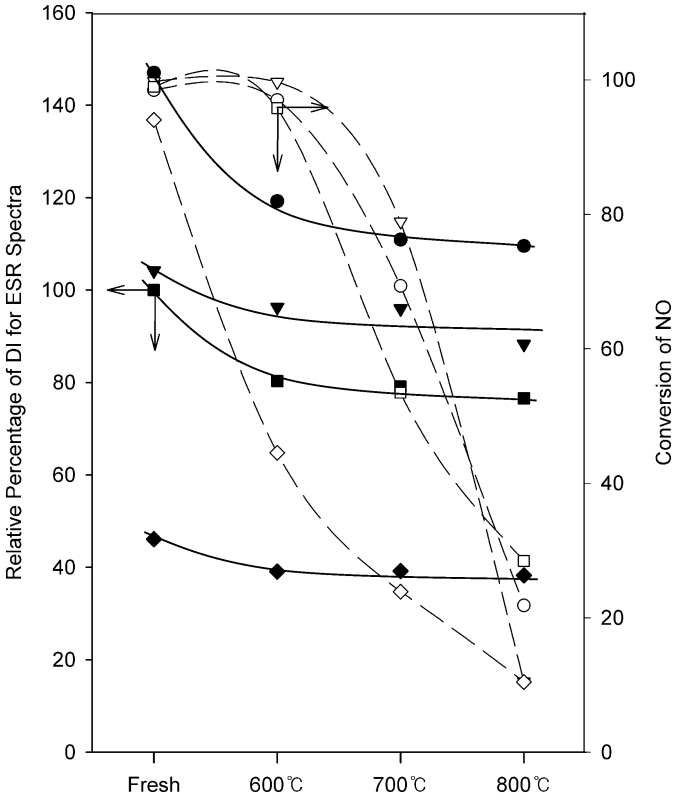

Fig. 11. Dependence of NO removal activity for a series of CuZSM5 catalysts on the relative percentage of DI value examined at 200 °C: Symbols for the relative percentage of DI value [(◆) CuZSM5-61, (■) CuZSM5-92, (▼) CuZSM5-124, (●) CuZSM5-150] and symbols for NO removal activity [(◇) CuZSM5-61, (□) CuZSM5-92, (▽) CuZSM5-124, (○) CuZSM5-150].

decreased slightly to 90–70% of their fresh counterparts as the result of hydrothermal aging.

Fig. 11 shows the relationship between relative DI value and NO removal activity at 200 °C, a typical reaction temperature (as shown in Fig. 3) for evaluating the effect of hydrothermal aging on the NO removal activity of the CuZSM5 catalysts for NH_3 SCR and urea SCR. No direct relationship between the amount of isolated Cu^{2+} species and NO removal activity of the catalyst was found. The NO conversion for CuZSM5-124-fresh was almost 100%, whereas the relative percentage of DI value was 104%, as shown in Table 4. But for CuZSM5-150-800, the NO conversion was only 22%, even though its relative DI value was 109%. Furthermore, NO conversion steeply decreased as the aging condition became more severe with respect to the sintering temperatures of 700 and 800 °C, even when the relative percentages of DI values for CuZSM5-92 and CuZSM5-124 remained nearly identical.

In particular, CuZSM5-61 catalysts exhibited much more severe catalyst aging than expected on the basis of the aging condition used, with negligible alterations of the amount and the electronic and geometric local structures of Cu^{2+} and BET and micropore surface areas as determined by XAFS, ESR, and N_2 adsorption. Although the relative percentage of DI values for CuZSM5-61-fresh was 46%, its NO conversion was almost 100%. However, the NO conversions of CuZSM5-61 and even CuZSM5-61-600 sharply decreased as the aging condition

Table 4
The relative percentage of DI value calculated from the ESR spectra for a series of CuZSM5 samples upon aging

Aging	Sample							
	CuZSM5-61		CuZSM5-92		CuZSM5-124		CuZSM5-150	
Fresh	46 (100)[a]	94[b]	100 (100)	99	104 (100)	100	153 (100)	98
600 °C	39 (85)	45	80 (80)	96	96 (92)	99	119 (78)	97
700 °C	39 (85)	24	79 (79)	53	96 (92)	79	110 (72)	69
800 °C	38 (83)	10	76 (76)	28	88 (85)	10	109 (71)	22

[a] The relative percentage of DI value calculated on the basis of the value of CuZSM5-92 arbitrarily set to be 100%. (The value in parentheses is the relative percentage of DI value based upon those of fresh samples.)

[b] NO removal activity of CuZSM5 catalysts at the reaction temperature of 200 °C.

became more severe. The NO conversion was at most 45%, even though the relative DI value hardly decreased compared with that of CuZSM5-61-fresh. This finding indicates that the decreased NO removal activity for underexchanged CuZSM5 catalysts may be essentially attributed to the migration of copper ions from active reaction sites—Cu^{2+} in a square planar (by $g_\parallel = 2.27$–2.30 and $A_\parallel = 150$–170 G of ESR signals) and square pyramidal ($g_\parallel = 2.33$–2.35 and $A_\parallel = 135$–145 G) environments—to less active sites—Cu^{2+} sites ($g_\parallel = 2.30$ and $A_\parallel = 165$ G, and $g_\parallel = 2.36$ and $A_\parallel = 130$ G) inaccessible to reactants such as NO, NH_3, etc. [20,22,24,43]. Furthermore, the substantial redistribution of Cu^{2+} sites on the surface of CuZSM5 during the course of hydrothermal aging may be expected to further interfere with the formation of active copper structure on the catalyst surface, such as oxygen-bridged oxocation $[Cu–O–Cu]^{2+}$ [14–16], due to poorly mobile Cu^{2+} ions.

For the overexchanged CuZSM5 catalysts, aging by hydrothermal treatment results from a decreased number of active reaction sites due to formation of bulk-type CuO and degradation of the ZSM5 support, as confirmed by surface area analyses and XRD. Moreover, for overexchanged catalysts, weaker migration of copper ions from the active reaction site (the square pyramidal and/or square planar Cu^{2+}) to two unresolved sites than occurs in underexchanged catalysts may be expected, because the active reaction sites on the surface of the overexchanged and/or 100% exchanged catalysts may be already full of Cu^{2+} ions, and no sites are available for the migration of the copper ions on catalyst aging. It may provide a guideline for ion exchange of the catalyst to optimize the copper content on the catalyst surface from the view of catalyst aging.

4. Conclusion

CuZSM5 has been reported as one of the most promising catalysts for the SCR of NO_x from light- and heavy-duty diesel engines with urea. However, the hydrothermal stability of the catalyst is another critical issue to be resolved for the commercial application of urea SCR technology to automotive engines. CuZSM5 after hydrothermal aging under simulated flue gas stream at temperatures above 600 °C with 10% water reveals significant catalyst deactivation. In particular, the worst deactivation was observed for underexchanged catalysts, even when a mild aging temperature at 600 °C was used. From XRD and

^{27}Al MAS-NMR analyses, no major alteration of the catalyst support due to dealumination has been observed by sintering. And the copper ions on the surface of the CuZSM5 catalysts remain as isolated Cu^{2+} and/or oxide form of copper confirmed by EXAFS. However, four distinctive local structures of Cu^{2+} species by ESR study exist on the surface of ZSM5 catalyst, such as the square pyramidal, the square planar, and two unresolved sites. The migration of the isolated Cu^{2+} ion from the square pyramidal and/or the square planar sites to unresolved sites occurs during hydrothermal aging, as confirmed by ESR spectra of the catalysts. It can be concluded that catalyst sintering of underexchanged CuZSM5 catalysts could be directly and indirectly attributed to the substantial redistribution of Cu^{2+} sites on the surface of CuZSM5 catalysts on the catalyst sintering. For the overexchanged CuZSM5 catalysts, the deactivation by hydrothermal treatment was associated with a combination of factors, including a decreased number of active reaction sites, isolated Cu^{2+} from the formation of bulk-type CuO, redistribution of Cu^{2+} sites, and structural degradation of the ZSM5 support, as confirmed by BET surface area analysis and XRD. It can be concluded that the optimal copper content for CuZSM5 catalysts to remove NO by urea is in the range of 3–4 wt% (nearly 125% ion-exchange level).

Acknowledgments

The authors are grateful to Pohang Light Source for the X-ray absorption spectroscopy measurements.

References

[1] M. Koebel, M. Elsener, M. Kleemann, Catal. Today 59 (2000) 335.
[2] L. Xu, R.W. McCabe, R.H. Hammerle, Appl. Catal. B 39 (2002) 51.
[3] J.H. Baik, S.D. Yim, I.-S. Nam, Y.S. Mok, J.-H. Lee, B.K. Cho, S.H. Oh, Top. Catal. 30/31 (2004) 37.
[4] I.-S. Nam, S.D. Yim, J.H. Baik, S.H. Oh, B.K. Cho, Korean Patent No. 10-0523287 (2005);
I.-S. Nam, S.D. Yim, J.H. Baik, S.H. Oh, B.K. Cho, US Patent Application 10/723,306 (2003).
[5] M.A. Larrubia, G. Ramis, G. Busca, Appl. Catal. B 27 (2000) L145.
[6] M. Kleemann, M. Elsener, M. Koebel, A. Wokaun, Ind. Eng. Chem. Res. 39 (2000) 4120.
[7] S.D. Yim, S.J. Kim, J.H. Baik, I.-S. Nam, Y.S. Mok, J.-H. Lee, B.K. Cho, S.H. Oh, Ind. Eng. Chem. Res. 43 (2004) 4856.
[8] T. Seiyama, T. Arakawa, T. Matsuda, Y. Takita, N. Yamazoe, J. Catal. 48 (1977) 1.
[9] M. Mizumoto, N. Yamazoe, T. Seiyama, J. Catal. 59 (1979) 319.
[10] W.B. Williamson, J.H. Lunsford, J. Phys. Chem. 80 (1976) 2664.
[11] N.D. Oates, J.H. Lunsford, J. Mol. Catal. 9 (1980) 91.
[12] M. Mizumoto, N. Yamazoe, T. Seiyama, J. Catal. 55 (1978) 119.
[13] E.-Y. Choi, I.-S. Nam, Y.G. Kim, J. Catal. 161 (1996) 597.
[14] T. Komatsu, M. Nunokawa, I.S. Moon, T. Takahara, S. Namba, T. Yashima, J. Catal. 148 (1994) 427.
[15] M. Iwamoto, H. Yahiro, K. Tanda, N. Mizuno, Y. Mine, S. Kagawat, J. Phys. Chem. 95 (1991) 3727.
[16] J. Sárkány, J.L. d'Itri, W.M.H. Sachtler, Catal. Lett. 16 (1992) 241.
[17] J. Ddeček, Z. Sobalík, Z. Tvarůžková, D. Kaucký, B. Wichterlová, J. Phys. Chem. 99 (1995) 16327.
[18] A.V. Kucherov, C.P. Hubbard, M. Shelef, J. Catal. 157 (1995) 603.
[19] S. Matsumoto, K. Yokota, H. Doi, M. Kimura, K. Sekizawa, S. Kasahara, Catal. Today 22 (1994) 127.
[20] T. Tanabe, T. Iijima, A. Koiwai, J. Mizuno, K. Yokota, A. Isogai, Appl. Catal. B 6 (1995) 145.
[21] Y. Yokomichi, T. Yamabe, H. Ohtsuka, T. Kakumoto, J. Phys. Chem. 100 (1996) 14424.
[22] G.T. Palomino, P. Fisicaro, S. Bordiga, A. Zecchina, E. Giamello, C. Lamberti, J. Phys. Chem. B 104 (2000) 4064.
[23] W. Gruenert, N.W. Hayes, R.W. Joyner, E.S. Shpiro, M.R.H. Siddiqui, G.N. Baeva, J. Phys. Chem. 98 (1994) 10832.
[24] S.A. Gómez, A. Campero, A. Martínez-Hernández, G.A. Fuentes, Appl. Catal. A 197 (2000) 157.
[25] J.O. Petunchi, W.K. Hall, Appl. Catal. B 3 (1994) 239.
[26] K.C.C. Kharas, H.J. Robota, D.J. Liu, Appl. Catal. B 2 (1993) 225.
[27] C. Torre-Abreu, M.F. Ribeiro, C. Henriques, F.R. Ribeiro, G. Delahay, Catal. Lett. 43 (1997) 31.
[28] J.Y. Yan, G.-D. Lei, W.H.M. Sachtler, H.H. Kung, J. Catal. 161 (1996) 43.
[29] B.K. Teo, EXAFS: Basic Principles and Data Analysis, Springer, Berlin, 1986.
[30] M. Newville, P. Livins, Y. Yacoby, J.J. Rehr, E.A. Stern, Phys. Rev. B 47 (1993) 14126.
[31] P.A. O'Day, J.J. Rehr, S.I. Zabinsky, G.E. Brown Jr., J. Am. Chem. Soc. 116 (1994) 2938.
[32] V.I. Parvulescu, P. Grange, B. Delmon, Catal. Today 46 (1998) 233.
[33] P. Marturano, L. Drozdova, A. Kogelbauer, R. Prins, J. Catal. 192 (2000) 236.
[34] S.M. Campbell, D.M. Bibby, J.M. Coddington, R.F. Howe, R.H. Meinhold, J. Catal. 161 (1996) 338.
[35] D.-J. Liu, H.J. Robota, J. Phys. Chem. B 103 (1999) 2755.
[36] H. Yamashita, M. Matsuoka, K. Tsuji, Y. Shioya, M. Anpo, M. Che, J. Phys. Chem. 100 (1996) 397.
[37] H. Hamada, N. Matsubayashi, H. Shimada, Y. Kintaichi, T. Ito, A. Nishijima, Catal. Lett. 5 (1990) 189.
[38] K.C.C. Kharas, D.-J. Liu, H. Robota, J. Catal. Today 26 (1995) 129.
[39] C. Lamberti, S. Bordiga, M. Salvalaggio, G. Spoto, A. Zecchina, F. Geobaldo, G. Vlaic, M. Bellatreccia, J. Phys. Chem. B 101 (1997) 344.
[40] R. Kumashiro, Y. Kuroda, M. Nagao, J. Phys. Chem. B 103 (1999) 89.
[41] S.C. Larsen, A. Aylor, A.T. Bell, J.A. Reimer, J. Phys. Chem. 98 (1994) 11533.
[42] A.V. Kucherov, H.G. Karge, R. Schlögl, Microporous Mesoporous Mater. 25 (1998) 7.
[43] M.W. Anderson, L. Kevan, J. Phys. Chem. 91 (1987) 4174.